IRSTI 29.19.37 https://doi.org/10.26577/phst20251219

Effect of copper in silver coatings on the corrosion behavior of NZ30K–0.1 wt.% ag alloy in Ringer–Locke solution

V. Greshta

Zaporizhzhia Polytechnic National University, Zaporizhzhia, Ukraine
e-mail: greshtaviktor@gmail.com
(*Received April 21, 2025; received in revised form May 30, 2025; accepted June 02, 2025*)

This study investigates the corrosion behavior of NZ30K + 0.1 wt.% Ag alloy coated with a silver layer containing copper impurities introduced unintentionally during plasma spraying. X-ray spectral analysis revealed the coating composition as 60.1 wt.% Ag and 39.9 wt.% Cu, which significantly influenced the corrosion performance in Ringer–Locke solution. Intense contact corrosion occurred at coating defects, initiating crevice corrosion and delamination at the transition between cylindrical and flat surfaces. A rapid negative shift in corrosion potential (E_{cor}) at 29.9 mV/s was observed–1.67 times faster than in samples with a 1200 nm thick pure silver coating. Subsequently, the shift rate decreased to 0.008 mV/s and stabilized at –1.356 V. Localized corrosion developed into pitting and deep ulcers due to selective anodic dissolution, resembling damage typical of stainless steels in chloride environments. The results indicate that copper contamination in silver coatings on NZ30K-based biodegradable implants is detrimental, as it accelerates local corrosion and hydrogen evolution, potentially contributing to muscle necrosis during bone healing.

Key words: Biodegradable magnesium alloy, NZ30K-Ag composite, corrosion in Ringer-Locke solution, copper-contaminated silver coatings, localized and crevice corrosion.
PACS number(s): 81.40.Np.

1 Introduction

Recently, biodegradable implants made of magnesium alloys have been used in traumatology [1]. Magnesium is not capable of forming self-protective oxide films [2], so its alloys with Al, Ca, Cu, Fe, Li, Mn, Ni, Sr, Zn [3-6], often modified with rare earth elements, are used to produce biodegradable implants for a controlled rate of their dissolution in the osteosynthesis process [7]. In addition, polymer coatings on the surface of biodegradable implants [8-12] and silver metallization [13] are often used to address these issues. In paper [14], NZ30K alloy additionally alloyed with 0.1 wt.% Ag was proposed for the production of biodegradable implants. It has high mechanical properties [15] and specific shock absorption capacity [16], which are required for such products [17], does not contain toxic chemical elements and does not contribute to biological complications, such as Alzheimer's disease, muscle destruction, and does not reduce osteoclast activity [18,19]. Zinc, Zr, and Nd in NZ30K alloy significantly reduce the rate of general corrosion (~50%) during osteosynthesis [20], but they form inclusions, intermetallic and other secondary phases, which in chloride-containing media, such as Ringer Locke solution, create microgalvanic pairs with a solid magnesium solution [21], which is the cause of pitting in the vicinity of these inclusions [22]. This is also inherent in stainless steels and alloys that are passivated [23-26]. In paper [27], it has been found that point and linear microdefects in the silver coating on the surface of the NZ30K alloy + 0.1 wt.% Ag were the focus of the nucleation of contact and crevice corrosion in the Ringer-Locke solution. They contributed to the local delamination of the coating from the alloy and the development of pitting and crevice corrosion, which proceeded according to the mechanisms established in [28-30]. At the same time, when silver is applied to the surface of the NZ30K+0.1 wt.% Ag alloy, it is possible that copper from the base on which the silver target is located may accidentally enter the coating. Under such conditions, copper can selectively dissolve in the silver coating. Therefore, the paper investigated the effect of copper in a silver coating on the surface of NZ30K+ 0.1 wt.% Ag alloy on its local corrosion destruction.

2 Materials and methods

We studied samples of silver-alloyed magnesium alloy NZ30K, which were smelted in an induction crucible furnace and subjected to aging [14]. The diameter of the samples was 12 and the length was 30 mm. Their chemical composition by the X-ray spectral method using the INKA ENERGY 350 has been determined (Table 1).

The samples of the alloy under study were clad with a 1300 nm thick layer of silver using a DC magnetron sputtering system equipped with a circular source and an Ag target (50 mm in diameter) in a gas discharge. The vacuum chamber of the system was a cylinder with an internal diameter and height of 500 mm. Cylindrical samples made of silver-alloyed NZ30K alloy + 0,1 mass. % (Table 1) were chemically degreased and cleaned by ultrasonication in a hot ethanol bath for 10 minutes and dried in warm air. Then they were mounted on a rotating (9 Hz) fixture located 90 mm from the sputtering source. Before deposition of the silver coating, air was pumped out of the chamber by a diffusion oil pump to a residual pressure of $1\text{-}10^{-3}$ Pa. The samples were ion-etched at a bias potential of 1000 V for 15 minutes at a pressure of 1.5 Pa. An unbalanced magnetron was used in a 600 mA DC mode at 400 V. The silver coating was applied at a constant magnetron power of 240 W and a base bias voltage of 100 V. The argon pressure in the deposition chamber was 1.0 Pa. The time of silver deposition on the surface of the studied magnesium alloy was 25 minutes for a coating thickness of 1300 nm.

Table 1 – Chemical composition of silver alloy NZ30K + 0,1 mass. % Ag.

Alloy	Content of chemical elements, wt. %				
NZ30K+Ag	Mg	Zn	Zr	Nd	Ag
	95.57	0.69	0.86	2.76	0.09

The chemical composition of the coating on the surface of the NZ30K alloy + 0.1 wt.% Ag was determined by X-ray spectroscopy using the INKA ENERGY 35, in particular, it has been determined that the silver content was 60.1 and copper was 39.9 wt. %.

Corrosion tests of silver clad samples with copper impurities have been carried out in a Ringer-Locke solution (an aqueous solution of undistilled water with the following chemical reagents, in mg/l NaCl – 9; $NaHCO_3$; $CaCl_3$; KCl 0.2; $C_6H_{12}O_6$ – 1) at a temperature of 20±1°C.

The establishment of the steady-state value of the corrosion potential E_{cor} on the tested samples on the PN-2MK-10A potentiostat in automatic mode has been recorded. The surface of the corrosion damage on the samples after their testing in the Ringer-Locke solution using an optical microscope MMR-2P and a scanning electron microscope JSM6360 with an energy dispersive microanalyzer JED-2300 has been examined.

3 Research results and discussion

According to the results of metallographic analysis of the surface of a sample made of NZ30K alloy + 0.1 wt.% Ag (Table 1) clad with a layer of silver and copper, last one accidentally got into it from a copper base for a silver target during plasma spraying, it has found that it has an ordered microstructure with micropores up to 0.1 μm in size (Fig. 1).

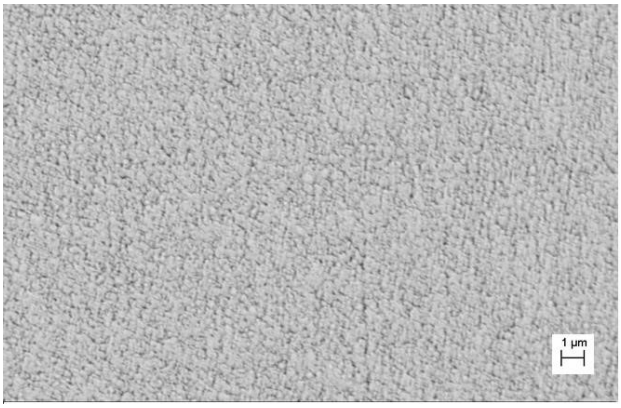

Figure 1 – Microstructure of a 1300 nm thick silver and copper clad layer on the surface of a NZ30K+0.1 wt.% Ag alloy sample (×1000).

It has been found that through these micropores in the coating, the NZ30K alloy + 0.1 wt.% Ag came into contact with the Ringer-Locke solution in which the sample has been tested. This caused contact corrosion on the end surface of the

sample (Fig. 2), which developed into crevice corrosion at the transition points of the end surface of the sample to the cylindrical surface and led to the formation of cracks in the coating and its delamination from the alloy (upper right corner of the sample, Fig. 2).

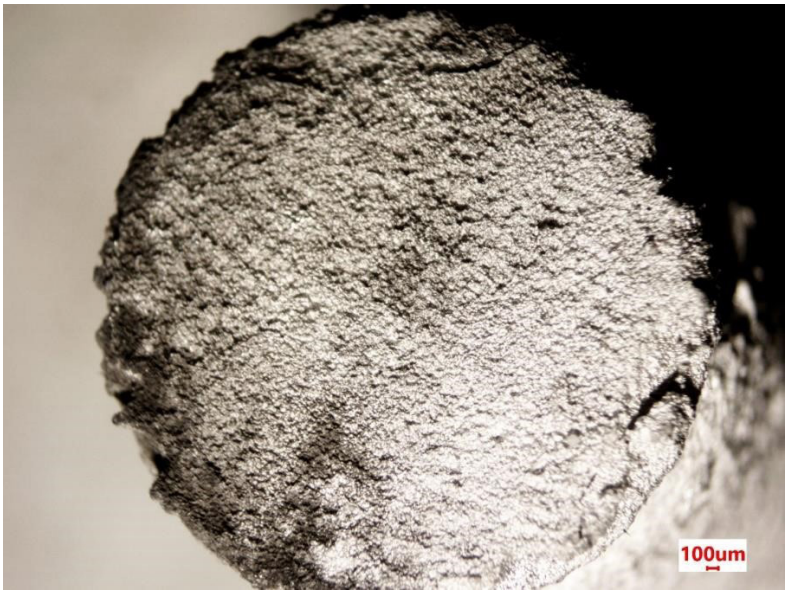

Figure 2 – End surface of a sample made of NZ30K alloy + 0.1 wt.% Ag clad with a layer of silver with copper impurities with a thickness of 1300 nm after corrosion tests in Ringer-Locke solution.

It should be noted that the cylindrical surface of the sample underwent more intense localized corrosion damage than the end surface (Fig. 3). Most likely, this is due to the technological features of coating on different surfaces of the sample and the state of their surfaces formed after casting and mechanical cutting of the end surface.

Figure 3 – Cylindrical surface of a sample made of NZ30K alloy + 0.1 wt.% Ag clad with a layer of silver with copper impurities with a thickness of 1300 nm after corrosion tests in Ringer-Locke solution.

Scanning electron microscopy of the surfaces of local corrosion damage of the studied sample (Figs. 2, 3) showed that they have a characteristic developed microrelief (Fig. 4) inherent in the selective dissolution of steels and alloys at the anode areas in corrosive media. This is consistent with the data of [31, 32].

Pores (~25 μm) and corrosion tunnels on the surface of the local corrosion damage of the test sample have been found (Fig. 4). According to [33], they can be formed as a result of the ionization of an electronegative chemical element on the surface of the alloy (Mg), which contributes to the formation of unbalanced vacancies that diffuse into its volume, where they coagulate and form pores. This tendency can be supported only by the solid-phase diffusion of magnesium atoms to the surface of local corrosion damage, as the chemical element with the most negative value of the standard electrode potential in the NZ30K alloy + 0.1 wt.% Ag, and Zn, Zr, Nd, and Ag in the opposite direction, since they are thermodynamically more stable than Mg [34, 35]. The observed (Figs. 2-4) local corrosion damage of the studied sample is characterized by critical potentials

(Table 2) at which its corrosion behavior has changed significantly, since (Fig. 4) shows the reorganization of the surface layers of the alloy with the formation of pores from corrosion tunnels that turned into corrosion ulcers. It should be noted that such mechanisms of formation of localized corrosion damage on the surface of samples of stainless steels and alloys were revealed in [28-30, 31, 36].

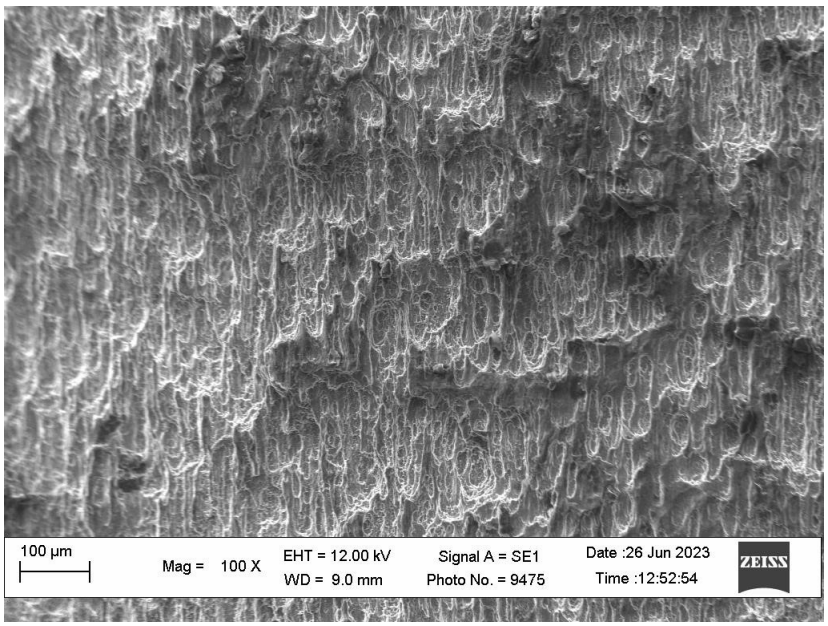

Figure 4 – Characteristic microrelief of the surface of local corrosion damage of a sample of NZ30K alloy + 0.1 wt.% Ag clad with a layer of silver with copper impurities with a thickness of 1300 nm after corrosion tests in Ringer-Locke solution.

Table 2 – Corrosion potentials E_{cor} of NZ30K alloy + 0.1 wt.% Ag clad with a layer of silver and copper 1300 nm thick depending on the time of exposure of samples in Ringer-Locke solution.

No. of points	τ, s	E_{cor}, V	No. of points	τ, s	E_{cor}, V	No. of points	τ, s	E_{cor}, V
1	4	-1.30944	21	300	-1.34432	41	1012	-1,3472
2	12	-1.31008	22	332	-1.34368	42	1044	-1,34912
3	20	-1.3104	23	364	-1.34432	43	1076	-1,34976
4	28	-1.31008	24	396	-1.34336	44	1140	-1,35328
5	36	-1.31136	25	428	-1.34368	45	1172	-1,35168
6	44	-1.31232	26	460	-1.344	46	1204	-1,35264
7	52	-1.31296	27	492	-1.344	47	1236	-1,35424
8	60	-1.31456	28	524	-1.34624	48	1268	-1.3536
9	68	-1.31488	29	556	-1.34528	49	1300	-1.35424
10	76	-1.31456	30	620	-1.3472	50	1364	-1.35328
11	84	-1.31456	31	652	-1.34784	51	1396	-1.35264
12	92	-1.31424	32	684	-1.3472	52	1428	-1.35296
13	100	-1.3152	33	716	-1.3456	53	1492	-1.35232
14	108	-1.31584	34	748	-1.3472	54	1524	-1.35264
15	116	-1.31648	35	780	-1.3472	55	1556	-1.35296

Continuation of the table

No. of points	τ, s	E_{cor}, V	No. of points	τ, s	E_{cor}, V	No. of points	τ, s	E_{cor}, V
16	124	-1.31584	36	812	-1.34784	56	1588	-1.35296
17	140	-1.3168	37	876	-1.34752	57	1652	-1.35488
18	148	-1.31744	38	908	-1.34624	58	1684	-1.35648
19	156	-1.31776	39	940	-1.3472	59	1748	-1.35616
20	172	-1.31808	40	972	-1.34912	60	1796	-1.35552

According to the results of the analysis (Fig. 5) and (Table 2), it has been found that after the first 156 seconds of testing, the potential of the sample under study shifted to the negative side at a rate of 0.1 mV/s. This is 1.67 times more intense than for a sample of the same alloy clad with a 1200 nm thick silver layer.

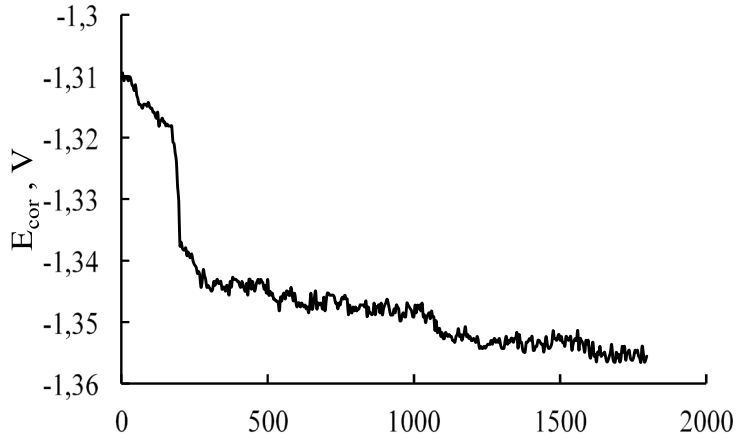

Figure 5 – Dependence between the corrosion potential E_{cor} of NZ30K alloy + 0.1 wt.% Ag clad with a layer of silver with copper impurities 1300 nm thick and the time of corrosion tests (τ) of the sample in Ringer-Locke solution.

Further, it has been recorded that the potential E_{cor} of the test sample abruptly shifted to the negative side from -1.31808 (point 20 after 172 seconds of testing (Table 2) to -1.344 V (points 26, 28 after 460 and 492 seconds of testing (Table 2) (Fig. 5). Thus, it has been found that the rate of shift of the potential E_{cor} of the sample to the negative side was 29.9 mV/s. This is due to the sudden detachment of a significant portion of the Ag+Cu clad layer from the alloy surface and a rapid increase in its contact area with the Ringer-Locke solution (Figs. 2, 3, 5). It should be noted that after that, a slow shift of the potential E_{cor} towards the negative side has been observed (Fig. 5). In particular, it shifted to the negative side from -1.34624 (point 28 after 524 seconds of testing (Table 2) to -1.35648 and -1.35616 V (points 58, 59 (Table 2). Thus, it turns out that the rate of this process was 0.008 mV/s and remained constant until the steady-state value of the corrosion potential E_{cor} of the sample has been established. A similar trend was observed for the sample of the NZ30K alloy + 0.1 wt. % Ag clad with a 1200-nm-thick silver layer. This shows that the copper in the silver coating intensifies contact corrosion between it and the alloy only at the first stage of testing, which accelerates its delamination and increases the area of contact between the alloy and the Ringer-Locke solution, which contributes to a rapid shift in the potential E_{cor} in the negative direction (Fig. 5). Further, the processes of corrosion dissolution of the sample proceeded according to the mechanisms inherent in the selective dissolution of steels and alloys at the anode areas [24, 32, 34, 36]. They determine the mechanisms of local anodic processes in alloys [28-30, 36], which depend on their

specific magnetic susceptibility, which determines the atomic state of the solid solution [37].

It should be noted that after immersion of the test sample in the Ringer-Locke solution, its potential E_{cor} was 62, 113, 124, and 109 mV higher than that of samples with coating thicknesses of 1200, 900, 500, and 200...300 nm, respectively. In addition, the difference between the steady-state values of corrosion potentials and those established after immersion of samples with a coating thickness of 1300 (Ag+Cu), 1200, 900, 500, and 200...300 nm (Ag) in the solution was 47, 55, 48, 32, and 27 mV, respectively. This may indicate that the intensity and duration of contact and crevice corrosion, which was accompanied by delamination of the coating from the alloy, was the lowest in samples with a coating thickness of 200...300 and 500 nm. At the same time, it should be noted that the potential difference found when establishing the steady-state values of corrosion potentials E_{cor} , for the sample with a coating thickness of 1300 nm (Ag+Cu) was even less than for the samples with 1200 and 900 nm, but the depth of local corrosion damage was the greatest. This is due to a decrease in cathodic depolarization under the influence of copper and an increase in the potential difference between the alloy and the coating. Thus, it can be noted that the presence of copper in the silver coating on the surface of implants is not permissible.

Summarizing the above, it can be noted that the sample of NZ30K+0.1 wt. % Ag clad with a 1300 nm thick layer of silver with copper impurities from the base on which the silver target for plasma spraying was placed, underwent intense contact and crevice corrosion with delamination of the coating at the intersection of cylindrical and flat surfaces. This contributed to the development of pitting and crevice corrosion of the sample under the influence of a chloride-containing media by mechanisms inherent in stainless steels and alloys. In addition, they were accelerated by the selective dissolution of copper in the silver coating.

4 Conclusion

According to the results of corrosion tests of a sample of NZ30K alloy + 0.1 wt. % Ag clad with layer of silver with copper impurities, it has been found that it was subjected to intense contact and crevice corrosion. It was accompanied by delamination of the coating from the alloy at the intersection of the cylindrical and end surfaces. In these places, pitting and ulcerative corrosion under the influence of a chloride-containing media was observed by mechanisms inherent in stainless steels and alloys. It is shown that the surfaces of corrosion pits on the studied sample have a characteristic microrelief inherent in the selective dissolution of metals on the anode areas of steels and alloys with pores (up to ~25 μm) formed as a result of the coagulation of nonequilibrium vacancies in the process of solid-phase diffusion of alloy components in their vicinity. It was found that the E_{cor} corrosion potential of the sample shifted to the negative side at a rate of 29.9 mV/s for 320 seconds, which is associated with localized coating delamination. Further, a slow negative shift of E_{cor} was observed at a rate of 0.008 mV/s until it reached a steady-state value of -1.356 V. It is proved that the presence of copper in the silver coating on the surface of implants is unacceptable.

References

1. Li H., Zheng Y., Qin L. Progress of biodegradable metals // Progress in natural science: Materials International. – 2014. – Vol. 24. – No. 5. – P. 414–422. https://doi.org/10.1016/j.pnsc.2014.08.014

2. Pilling N., Bedworth R.J. The oxidation of metals at high temperatures // Inst. Metals. – 1993. – Vol. 29. – P. 529–593.

3. Müller W.D., Nascimento M.L., Zeddies M., Córsico M., Gassa L.M., Mele M.A.F.L.D. Magnesium and its alloys as degradable biomaterials: corrosion studies using potentiodynamic and EIS electrochemical techniques // Materials Research. – 2007. – Vol. 10. – P. 5–10. https://doi.org/10.1590/S1516-14392007000100003

4. Witte F., Ulrich H., Rudert M., Willbold E. Biodegradable magnesium scaffolds: Part 1: Appropriate inflammatory response // Journal of Biomedical Materials Research Part A. – 2007. – Vol. 81. – P. 748–756. https://doi.org/10.1002/jbm.a.31170

5. Xu L., Yu G., Zhang E., Pan F., Yang K. In vivo corrosion behavior of Mg–Mn–Zn alloy for bone implant application // Journal of Biomedical Materials Research Part A. – 2007. – Vol. 83, No. 3. – P. 703–711. https://doi.org/10.1002/jbm.a.31273

6. Zhang G.D., Huang J.J., Yang K., Zhang B.C., Ai H.J. Experimental study of in vivo implantation of a magnesium alloy at early stage // Acta Metallurgica Sinica. – 2007. – Vol. 43. – P. 1186–1190.

7. Mueller W.-D., Nascimento M.L., Zeddies M., Corsico M., Gassa L.M., de Mele M.F.L. Magnesium and its alloys as degradable biomaterials: corrosion studies using potentiodynamic and EIS electrochemical techniques // Materials Research. – 2007. – Vol. 10, No. 1. – P. 5–10. http://dx.doi.org/10.1590/S1516-14392007000100003

8. Komarov F.F., Ismailova G.A., Mil'chanin O.V., et al. Effect of thermal processing on the structure and optical properties of crystalline silicon with GaSb nanocrystals formed with the aid of high-dose ion implantation // Technical Physics. – 2019. – Vol. 60. – P. 1348–1352. http://dx.doi.org/10.1134/S1063784215090078

9. Muradov A.D., Mukashev K.M., Korobova N.E., et al. Influence of γ-Irradiation on the Optical Properties of the Polyimide–$YBa_2Cu_3O_{6.7}$ System // Journal of Applied Spectroscopy. – 2018. – Vol. 85. – P. 260–266. http://dx.doi.org/10.1007/s10812-018-0642-4

10. Sagyndykov A.B., Kalkozova Z.K., et al. Fabrication of nanostructured silicon surface using selective chemical etching // Technical Physics. – 2017. – Vol. 62. – P. 1675–1678. http://dx.doi.org/10.1134/S106378421711024X

11. Muradov A., Mukashev K., Ismailova G., et al. Chemical co-precipitation synthesis and characterization of polyethylene glycol coated iron oxide nanoparticles for biomedical applications // Int. Multidisc. Sc. GeoConf. SGEM. – 2017. – Vol. 17. – P. 201–208. http://dx.doi.org/10.5593/sgem2017/61/S24.027

12. Yar-Mukhamedova G.S., Darisheva A.M., Yar-Mukhamedov E.S. Adsorption of the components of a chrome-plating electrolyte on dispersed corundum particles // Materials Science. – 2019. – Vol. 54. – P. 907–912.

13. Muradov A.D., Mukashev K.M., Korobova N.E. Impact of silver metallization and electron irradiation on the mechanical deformation of polyimide films // Technical Physics. – 2017. – Vol. 62, No. 11. – P. 1692–1697. http://dx.doi.org/10.1134/S1063784217110226

14. Greshta V.L., Shalomeev V.A., Dzhus A.V., Mityaev O.A. Study of the effect of silver alloying on the microstructure and properties of magnesium alloy NZ30K for implants in osteosynthesis // New Materials and Technologies in Metallurgy and Engineering. – 2023. – Vol. 2. – P. 14–19. https://doi.org/10.15588/1607-6885-2023-2-2

15. Zhou H., Hou R., Yang J., Sheng Y., Li Z., Chen L., Li W., Chen L., Li W., Wang X. Influence of Zirconium (Zr) on the microstructure, mechanical properties and corrosion behavior of biodegradable zinc-magnesium alloys // Journal of Alloys and Compounds. – 2020. – Vol. 840. – P. 155792. https://doi.org/10.1016/j.jallcom.2020.155792

16. Sun M., Yang D., Zhang Y., Mao L., Li X., Pang S. Recent advances in the grain refinement effects of Zr on Mg alloys: a review // Metals. – 2022. – Vol. 12, No. 8. – P. 1388. https://doi.org/10.3390/met12081388

17. Wang J., Zou Y., Dang C., Wan Z., Wang J., Pan P. Research progress and the prospect of damping magnesium alloys // Materials. – 2024. – Vol. 17, No. 6. – P. 1285. https://doi.org/10.3390/ma17061285

18. Ferreira P.C., Piai K.D.A., Takayanagui A.M.M., Segura-Muñoz S.I. Aluminum as a risk factor for Alzheimer's disease // Revista Latino-Americana de Enfermagem. – 2008. – Vol. 16. – P. 151–157. https://doi.org/10.1590/S0104-11692008000100023

19. Bach F.W., Schaper M., Jaschik C. Influence of lithium on hcp magnesium alloys // Materials Science Forum. – 2003. – Vol. 419. – P. 1037–1042.

20. Sun M., Wu G., Wang W., Ding W. Effect of Zr on the microstructure, mechanical properties and corrosion resistance of Mg-10Gd-3Y magnesium alloy // Materials Science and Engineering: A. – 2009. – Vol. 523, No. 1–2. – P. 145–151. https://doi.org/10.1016/j.msea.2009.06.002

21. Zeng R.-C., Zhang J., Huang W.-J. et al. (2016) Review of studies on corrosion of magnesium alloys // Transactions of Nonferrous Metals Society of China. – Vol. 16, No. 2. – P. 763–771. https://doi.org/10.1016/S1003-6326(06)60297-5

22. Ghali E. Properties, use and performance of magnesium and its alloys // Corrosion Resistance of Aluminum and Magnesium Alloys: Understanding, Performance and Testing. –2020. – P. 319–347. https://doi.org/10.1002/9780470531778

23. Narivs'kyi O.E. Corrosion fracture of platelike heat exchangers // Fiziko-Khimichna Mekhanika Materialiv. – 2005. -Vol. 41, No. 1. – P. 104–108. https://www.scopus.com/record/display.uri?eid=2-s2.0-27744440620

24. Narivs'kyi O. The influence of heterogeneity of AISI321 steel on its pitting resistance in chloride-containing media // Materials Science. – 2007. -Vol. 43, No. 2. – P. 256–264. https://doi.org/10.1007/s11003-007-0029-9

25. Narivskiy A., Yar-Mukhamedova G., Temirgaliyeva E. et al. Corrosion losses of alloy 06KhN28MDT in chloride-containing commercial waters // Int. Multidisc. Sc. GeoConf. SGEM. – 2016. -P. 63–70.

26. Mishchenko V.G., Snizhnoi G.V., Narivs'kyy O.E. Magnetometric investigations of corrosion behavior of AISI 304 steel in chloride-containing environment // Metallofizika i Noveishie Tekhnologii. – 2011. -Vol. 33, No. 6. – P. 769–774.

27. Greshta V., Narivskyi O., Dzhus A. et al. Corrosion dissolution of an implant made of NZ30K alloy alloyed with Ag and coated with a layer of silver in a model solution of the osteosynthesis process // Int. Multidisc. Sc. GeoConf. SGEM. -2024. -P. 1.

28. Narivskyi O.E., Subbotin S.O., Pulina T.V. et al. Modeling of pitting of heat exchangers made of 18/10 type steel in circulating waters // Materials Science. – 2023. -Vol. 58, No. 5. – P. 1–7. https://doi.org/10.1007/s11003-023-00725-y

29. Narivskyi O.E., Subbotin S.O., Pulina T.V. et al. Mechanism of pitting corrosion of austenitic steels of heat exchangers in circulating waters and its prediction // Materials Science. –2023. -Vol. 59, No. 5. – P. 275–282. https://doi.org/10.1007/s11003-024-00773-y

30. Narivskyi O., Subbotin S., Pulina T. Corrosion behavior of austenitic steels in chloride-containing media during the operation of plate-like heat exchangers // Physical Sciences and Technology. – 2023. -Vol. 10, No. 3–4. – P. 48–56. https://doi.org/10.26577/phst.2023.v10.i2.06

31. Narivs'kyi O.E. Micromechanism of corrosion fracture of the plates of heat exchangers // Materials Science. – 2007. -Vol. 43, No. 1. – P. 124–132. https://doi.org/10.1007/s11003-007-0014-3

32. Narivs'kyi O.E. Corrosion fracture of platelike heat exchangers // Materials Science. – 2005. -Vol. 41, No. 1. – P. 122–128. https://doi.org/10.1007/s11003005-0140-8

33. Pickering H.W. Characteristic features of alloy polarization curves // Corrosion Science. – 1983. -Vol. 23, No. 10. – P. 1107–1120. https://doi.org/10.1016/0010-938X(83)90092-6

34. Poutbaix M., De Zoubov N. Atlas of electrochemical equilibrium in aqueous solutions. – Pergamon Press. -1966. https://doi.org/10.1016/0022-0728(67)80059-7

35. Moffat T.P., Fan F.-R.F., Bord A.J. Electrochemical and scanning tunneling microscopic study of dealloying of Cu_3Au // Electrochemical Society. – 1991. -Vol. 11. – P. 3224–3235.

36. Narivs'kyi O.E., Belikov S.B. Pitting resistance of 06KhN28MDT alloy in chloride-containing media // Materials Science. – 2008. -Vol. 44. – P. 573–580. https://doi.org/10.1007/s11003-009-9107-5

37. Narivs'kyi O.E., Snizhnoi G.V., Pulina T.V. et al. Effect of specific magnetic susceptibility of AISI 304 and 08Kh18N10 steels on their limiting potentials in chloride-containing environments // Materials Science. – 2024. -Vol. 59, No. 3. – P. 649–657. https://doi. org/10.1007/s11003-024-00824-4

38. Dzhus A., Subbotin S., Pulina T., Snizhnoi G. Modeling the resistance of plate-like heat exchangers made of 06KhN28MDT alloy (analogous to AISI 904L steel) to crevice corrosion in recycled water enterprises // Physical Sciences and Technology. – 2024. -Vol. 11, No. 3–4. – P. 58–66. https://doi.org/10.26577/phst2024v11i2b07

39. Zellele D.M., Yar-Mukhamedova G.Sh., Rutkowska-Gorczyca M.A. A review on properties of electrodeposited nickel composite coatings: Ni-Al_2O_3, Ni-SiC, Ni-ZrO_2, Ni-TiO_2 and Ni-WC // Materials. –2024. -Vol. 17, No. 23. – P. 5715. https://doi. org/10.3390/ma17235715

40. Imanbayeva A.K., Syzdykova R.N., Temirbayev A.A. Concept formulation and university teaching methodology for dynamic chaos // Journal of Physics: Conference Series. – Vol. 1136, No. 1. – P. 012029. https://doi.org/10.1088/1742-6596/1136/1/012029

41. Prikhodko O., Maltekbasov M., Almasov N. et al. Structure and electronic properties of amorphous $As_{40}Se_{30}S_{30}$ films prepared by ion-plasma sputtering method // Physical Sciences and Technology. –2016. – Vol. 2, No. 1. https://doi.org/10.26577/2409-6121-2015-2-1-24-29

42. Zelele D.M., Rutkowska-Gorczyca M. Electrochemical synthesis and functional properties of metal and alloy-based composition coatings // Recent Contributions to Physics. –2024. -Vol. 1, No. 88. – P. 41–48.

43. Greshta V., Narivskyi O., Dzhus A. et al. Corrosion behaviour of magnesium alloys NZ30K and NZ30K alloyed with silver in the model solution of the osteosynthesis process // Eurasian Physical Technical Journal. –2024. -Vol. 21, No. 3. – P. 29–36. https://doi.org/10.31489/2024No3/29-36

44. Mussabek G.K., Yermukhamed D., Dikhanbayev K.K. et al. Self-organization growth of Ge-nanocolumns // Materials Research Express. –2017. -Vol. 4. – P. 035003. https://doi.org/10.1088/2053-1591/aa5ed6

45. Sakhnenko N., Ved M., Koziar M. Ternary cobalt-molybdenum-zirconium coatings: electrolytic deposition and functional properties // Physical Sciences and Technology. –2018. – Vol. 3, No. 2. – P. 65–75. https://doi.org/10.26577/phst-2016-2-108

46. Imanbayeva A., Tursynbek Y., Syzdykova R., Mukhamedova A. Evaluating the effectiveness of information security based on the calculation of information entropy // Journal of Physics: Conference Series. -2021. -Vol. 1783(1). -Art. 012042. https://doi.org/10.1088/1742-6596/1783/1/012042

47. Mussabek G., Zhylkybayeva N., Lysenko I., Lishchuk P.O., Baktygerey S., Yermukhamed D., Taurbayev Ye., Sadykov G., Zaderko A.N., Skryshevsky V.A., Lisnyak V.V., Lysenko V. Photo- and radiofrequency-induced heating of photoluminescent colloidal carbon dots // Nanomaterials. -2022. -Vol.12. – Art. 2426. https://doi.org/10.3390/nano12142426

48. Yar-Mukhamedova G., Muradov A., Mukashev K., Umarov F., Imanbayeva A., Mussabek G., Belisarova F. Impact of polyethylene terephthalate on the mechanical properties of polyimide films // Eurasian Physical Technical Journal. -2025. -Vol. 22, 28–36. https://doi.org/10.31489/2025N1/28-36

49. Nenastina T., Sakhnenko M., Oksak S., Yar-Mukhamedova G., Zellele D., Mussabek G., Imanbayeva A. Study of complexation patterns in the system Ni^{2+}, MoO_4^{2-}, $P_2O_7^{4-}$, Cit^{3-} for the development of poly-ligand electrolytes // Eurasian Chemico-Technological Journal. -2024. -Vol. 26. -P. 155–160. https://doi.org/10.18321/ectj1638

50. Muradov A., Młyniec A., Mukashev K., Yar-Mukhamedova G., Sandybaev Y. Simulation of mechanical strain of metallic electron-irradiated polyimide films // Physical Sciences and Technology. -2018. -Vol. 4(2). -P. 95–100. https://doi.org/10.26577/phst-2017-2-139

Information about author:

Greshta Victor L., Candidate of Technical Sciences, Professor at the Zaporizhzhia Polytechnic National University, Zaporizhzhia, Ukraine; email: greshtaviktor@gmail.com.